ACS APPLIED MATERIALS & INTERFACES

Research Article

www.acsami.org

Facile, One-Pot Synthesis, and Antibacterial Activity of Mesoporous Silica Nanoparticles Decorated with Well-Dispersed Silver Nanoparticles

Yue Tian,[‡,§] Juanjuan Qi,[‡,†] Wei Zhang,*[,‡] Qiang Cai,*[,†] and Xingyu Jiang*[,‡]

[‡]Beijing Engineering Research Center for BioNanotechnology and CAS Key Lab for Biological Effects of Nanomaterials and Nanosafety, National Center for Nanoscience and Technology, Beijing 100190, China

[†]Department of Materials Science and Engineering, Tsinghua University, Beijing 100084, China

[§]University of Chinese Academy of Sciences, Beijing 100049, China

Supporting Information

ABSTRACT: In this study, we exploit a facile, one-pot method to prepare MCM-41 type mesoporous silica nanoparticles decorated with silver nanoparticles (Ag-MSNs). Silver nanoparticles with diameter of 2−10 nm are highly dispersed in the framework of mesoporous silica nanoparticles. These Ag-MSNs possess an enhanced antibacterial effect against both Gram-positive and Gram-negative bacteria by preventing the aggregation of silver nanoparticles and continuously releasing silver ions for one month. The cytotoxicity assay indicates that the effective antibacterial concentration of Ag-MSNs shows little effect on human cells. This report describes an efficient and economical route to synthesize mesoporous silica nanoparticles with uniform silver nanoparticles, and these nanoparticles show promising applications as antibiotics.

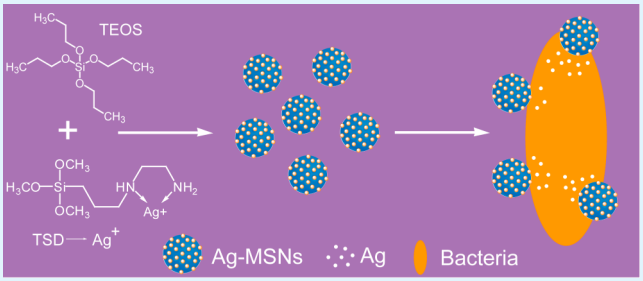

KEYWORDS: *mesoporous silica nanoparticles, silver nanoparticles, antibacterial activity, continuously release, highly dispersity*

INTRODUCTION

Silver nanoparticles (Ag NPs) have shown efficient and broad-spectrum antibacterial activity compared to other metal materials.[1−4] Nevertheless, practical applications of Ag NPs are often hampered by oxidization of these nanoparticles, which may cause aggregation and loss of antibacterial activity.[5−7] To solve these problems, several inorganic carriers, such as zeolite,[8] titanium dioxide,[9,10] activated carbon,[11] and montmorillonite,[12] have been investigated as silver-carrying antibacterial agents. Silver can be added to these carriers by electrostatic binding, physical adsorption, or cation exchange. Such composites can effectively enhance the antibacterial activity and reduce preparation cost. However, unfavorable biocompatibility, large size, and low dispersity of these composites limit their practical applications.[13−16]

Since Beck et al.[17] reported their pioneering work in 1992, MCM-41 type mesoporous silica nanoparticles (MSNs) have attracted great attention for their uniform porous structure, tunable porous diameters between 2 and 50 nm, high chemical and thermal stability, and large surface area. In particular, applications of these nanoparticles in biomedicine have been widely investigated.[18−26] Owing to the biocompatibility[22] and the functional versatility of MCM-41 type MSNs[21,27] (simplicity in modifying both particles and pores), these materials have been successfully used for drug delivery applications,[23,28] controlled release systems for drugs,[24] and antimicrobial carriers (encapsulated antibacterial agents).[29]

As Ag NPs can be easily embedded within silica nanoparticles to form Ag-containing materials which can protect Ag NPs from aggregation and can slowly release Ag ions, these materials are predicted to have a more effective application in antibacterial field than conventional Ag NPs. Recently, some efforts focused on the development of core−shell structures by using silicon to coat Ag NP cores.[30,31] These core−shell systems can effectively protect active Ag NPs and achieve superior antibacterial activities.[25] Another strategy to load Ag NPs is to directly deposit them on the surface of silicon materials.[32] The supporting matrix can prevent Ag NPs aggregation and the composites can release Ag ions to realize antibacterial effects.[33] In the Si−Ag systems, the steady release of silver ions from silver nanoparticles is a critical factor to the antimicrobial function of Ag NPs, so the uniform distribution of silver nanoparticles with small sizes on silicon substrate should be considered prior to synthesis.[34] But in most of the previous studies, Ag NPs were either completely wrapped in the cores or just dispersed on the surface of mesoporous silica. The antibacterial ability of Ag NPs in core−shell Ag-silica composite

Received: February 20, 2014
Accepted: July 22, 2014
Published: July 22, 2014

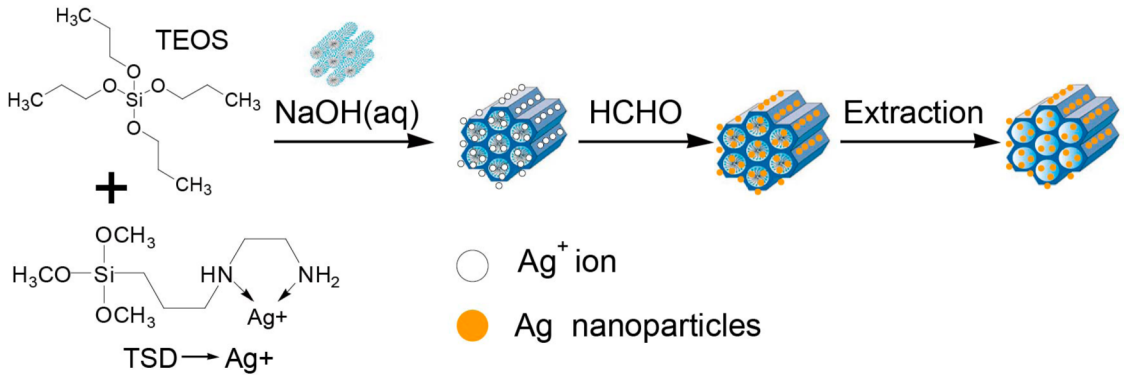

Figure 1. Formation schematics of Ag-MSNs by the co-condensation of TEOS and TSD in extremely dilute sodium hydroxide solution.

material cannot be fully utilized due to its slow Ag ion release rate. Ag NPs, which are just loaded on to the surface of the silica, may be quickly consumed, resulting in a rapid decrease of antibacterial activity due to the weak binding or chemical erosion. In addition, in most of these cases, the decorated Ag NPs require a separate synthesis, so the preparation of the Si−Ag system needs at least a two-step synthesis. In addition, Ag NPs with smaller size are proven to exhibit higher antibacterial activity. However, the size of Ag NPs in many Si−Ag systems is larger than 20 nm. Hence, it is necessary to design a convenient synthetic method and a new structure of Ag-silica composite to get better antibacterial performance.

In the present study, we focus on the facile preparation of MCM-41 type MSNs decorated with silver nanoparticles (Ag-MSNs) by the co-condensation method in extremely dilute sodium hydroxide solution, and test the antimicrobial activity of the materials against bacteria. This straightforward method does not need prior synthesis of Ag NPs or silica NPs; silica NPs decorated with Ag NPs can be synthesized by a one-pot and green synthetic route. This method also makes the small size of Ag NPs highly disperse in the framework of MCM-41 type MSNs. These nanoparticles can effectively prevent the aggregation of Ag NPs and continuously release Ag ions, inducing long-term antibacterial activity against both Gram-negative and Gram-positive bacteria. Furthermore, the effective antibacterial concentration of Ag-MSNs exhibits little toxic effect on human endothelial cells. Given that stable Ag NPs can readily decorate MCM-41 type MSNs, we conclude that this process could provide a facile and environmentally friendly approach to develop antibacterial materials with good biocompatibility.

MATERIALS AND METHODS

Materials. In this study, hexadecyltrimethylammonium bromide (CTAB), tetraethylorthosilicate (TEOS), sodium hydroxide (NaOH), silver nitrate ($AgNO_3$), formalin (HCHO, 37%), methanol (CH_3OH), ethanol (C_2H_5OH), and ammonium nitrate (NH_4NO_3) were purchased from Beijing Chemical Plant. Coupling agent *N*-(amino-ethyl)-amino-propyl trimethoxysilane (TSD) was purchased from Aladdin-reagent Company. All chemicals were analytic grade, and used without further purification. AgNPs were obtained from Sigma-Aldrich (10 nm particle size, sodium citrate as stabilizer, the measurement potential is −9 mV). The deionized water (H_2O) with an electrical conductivity larger than 7 MΩ was used as the solvent. Standard strains of *Escherichia coli* ATCC 11775, *Staphyloccocus aureus* ATCC 6538P were purchased from China General Microbiological Culture Collection Center.

Synthesis of Ag-MSNs. MCM-41 decorated with silver nanoparticles were prepared via a modified Cai reaction[35] (Figure 1). In a typical reaction, solution A (0.3 g CTAB dissolved in 110 mL deionized water, 1 mL NaOH (2 M) was added with stirring and heating at 75 °C); solution B (2 mL TEOS dissolved in 10 mL methanol); and solution C (0.06 g $AgNO_3$ was mixed with 10 mL deionized water with stirring, 0.5 mL of TSD was added after 10 min) were prepared. Eight milliliters of solution B was added dropwise into solution A and reacted for 15 min under vigorous stirring to form mesoporous silica cores. Solution C and the remaining solution B were added dropwise into solution A (TEOS and TSD as co-condensation precursors) (see Figure 1), with stirring for an additional 2 h. Finally, 5 mL of formalin was added dropwise into the mixture with stirring for an additional 1 h to reduce Ag ions into Ag NPs, collected by centrifugation, and washed with ethanol. The CTAB extraction was performed by adding the as-prepared nanoparticles in a solution of ethanol (100 mL) and ammonium nitrate (0.3 g) followed by stirring at 60 °C for 10 h. The extracted samples were thoroughly washed with deionized water.

Characterization of Ag-MSNs. Sample morphology, microstructure, and distribution of Ag NPs were examined by scanning electron microscopy (SEM, HITACHI S-4500 scanned electron microscope, Japan), high resolution transmission electron microscopy (HRTEM, JEM-200CX transmission electron microscope operated at 200 kV, Japan), transmission electron microscopy (TEM, JEM-200CX transmission electron microscope operated at 200 kV, Japan), and high-angle annular dark-field scanning transmission electron microscopy (HAADF-STEM, Tecnai G2 F20 U-TWIN field emission transmission electron microscope, America). Zeta potential of the sample is analyzed by a Zetasizer Nano ZS (Malvern Company, England). For TEM analysis, specimens were prepared by dispersing the as-obtained powder in alcohol and then dipping a drop of the suspension on a copper grid coated with transparent graphite, followed by drying. To investigate the position of the loading Ag NPs, a cross-section of Ag-MSNs was prepared. The samples were embeded in epoxy and ultrathin sections of Ag-MSNs were microtomed with a diamond knife. The cross sections of Ag-MSNs were collected on copper grids for TEM observation. To investigate the structure and crystallinity of the samples, the powders were further analyzed with an X-ray powder diffractometer (XRD, Rigaku D/max-rA diffractometer with Cu Kα radiation (λ = 1.5418 Å) at 40 kV, 200 mA, Japan). The sample was scanned from 0.6° to 10° (2θ) with a step size of 0.02° and a count time of 1 s at each point. A nitrogen adsorption instrument (Micrometritics ASAP2020) was applied to study the Brunauer−Emmett−Teller (BET) surface area and the porosity of the samples. The UV/vis spectra were measured with UV2450 spectrophotometer (Shimadzu) over the wavelength range from 300 to 800 nm. Measurement of ICP-MS provided quantitative evidence that the Ag content in Ag-MSNs is about 4.2%.

Antibacterial Properties. *Escherichia coli* (*E. coli*) and *Staphyloccocus aureus* (*S. aureus*) were selected as model Gram-negative and Gram-positive bacteria to study the antibacterial activity of Ag-MSNs. Bacteria were cultured in the Luria−Bertani (LB) medium (10 g/L casein tryptone, 5 g/L yeast extract, and 10 g/L NaCl, pH = 7) at 37 °C on a shaker bed at 200 rpm.

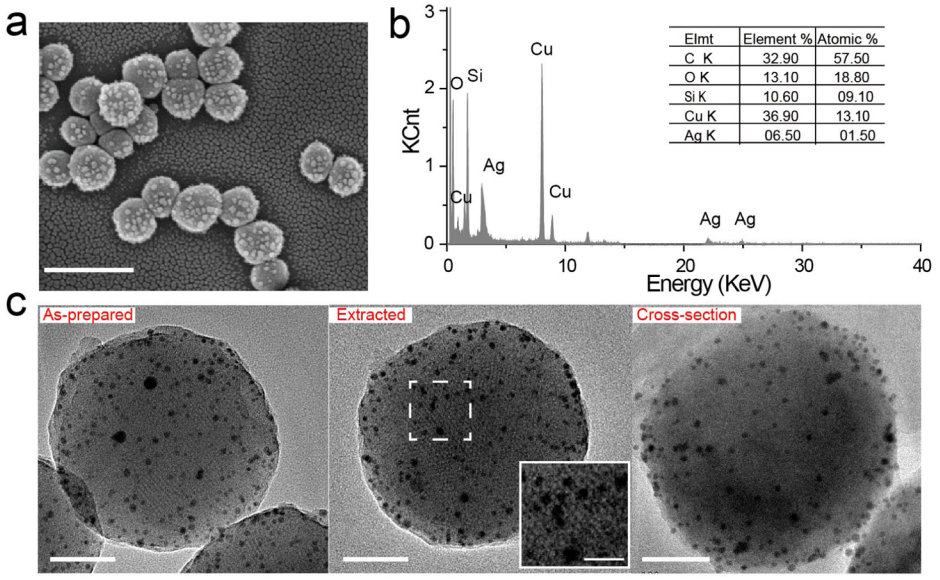

Figure 2. Characterization of Ag-MSNs: (a) SEM image of Ag-MSNs. Scale bar: 500 nm. (b) Pattern of EDX elemental analysis of Ag-MSNs. (c) HRTEM images of the as-prepared Ag-MSNs and extracted Ag-MSNs, and cross-section TEM images of Ag-MSNs. Scale bars: left (50 nm); middle (50 nm); right (100 nm). The picture inside the white box showed that Ag-MSNs still contain parallel channels after removal of CTAB. Scale bar: 20 nm.

Bacterial Kinetic Test. Ag-MSNs with different concentrations (0−320 μg/mL) were prepared in each sterilized flask and inoculated with 1×10^6 CFU/mL bacteria suspension. Commercial Ag NPs and PBS were used as controls. The initial time of adding bacteria suspension to each sample was taken as zero, and fractions of suspension (100 μL) were withdrawn from the flasks at set time intervals. Immediately, these aliquots were transferred to a Corning 96-well plate for the determination of $OD_{600\ nm}$ using Tecan infinite 200 multimode microplate readers to count bacterial colonies. Cultures were prepared in triplicate, and all experiments were repeated twice. The pictures of bacteria treated with 0−320 μg/mL Ag-MSNs at different time points were photographed with an Olympus digital camera (S320) and commercial Ag NPs, $AgNO_3$, and PBS were used as controls.

LB-Agar Plates. The Ag-MSNs nanoparticles were mixed with molten LB-agar medium at various final concentrations (0−320 μg/mL). Commercial Ag NPs, $AgNO_3$, and PBS were used as controls. After the agar was cooled to room temperature, serial dilution ($1/10^4$) of late log phase bacteria were then plated onto the above agar plates and incubated at 37 °C. The bactericidal activity of Ag-MSNs was also determined by LB-agar plates. 1×10^6 CFU/mL *E. coli* or *S. aureus* was incubated with 80 or 320 μg/mL Ag-MSNs, followed by plating 100 μL of the complex onto the agar plate at intervals and counting the number of bacterial colonies after 24 h incubation.

Characterization of Bacteria after Treatment with Ag-MSNs or Ag NPs. The size and morphology of Ag-MSNs or Ag NPs incubated with bacteria were examined by TEM and STEM. Prior to microscopy analysis, bacteria samples were treated using standard procedures for fixing and dehydrating biological samples, which are described in previous literature.[36,37]

Measurement of Released Ag Content in Ag-MSNs. The concentration of released Ag from Ag-MSNs was tested using dialysis tubes. A mass of 0.3 g of the powdered product was dissolved in 5 mL water and this solution was filled in a dialysis tube (Spectra/Por Biotech; cellulose ester; MWCO 14000). This dialysis tube was immersed in 900 mL of ultrapure water. The process of dialysis was carried out under continuous stirring at 37 °C. At selected intervals, 5 mL solution outside the dialysis tube was taken out and the same amount of water was added. The Ag content in the samples was measured using inductively coupled plasma−mass spectrometry (ICP-MS, Elan5000, PE-Sciex, America). The release of Ag from Ag-MSNs and commercial Ag NPs in LB culture medium is similar to the above method, and water changed to LB medium.

Cellular Toxicity Evaluation. The *in vitro* cytotoxicity was evaluated by cell counting kit (CCK). Human umbilical vein endothelial cells (HUVECs) were purchased from American Type Culture Collection (ATCC, USA). Cells were seeded into a 96-well plate at a concentration of 1×10^4 cells/well in 100 μL DMEM culture medium supplemented with 10% FBS, 100 U/mL penicillin, and 100 μg/mL streptomycin. Twenty-four hours postseeding, all samples (80, 320, and 476 μg/mL Ag-MSNs, 20 μg/mL Ag NPs, 31 μg/mL $AgNO_3$, and 476 μg/mL MSNs) were added to each well (five wells for each sample). Cells without any treatment were used as the control. The CCK assays were performed after a culture time of 24, 48, and 72 h. After 4 h incubation at 37 °C, the absorbance at 450 nm (with reference wavelength of 620 nm) of each well was measured by Tecan infinite 200 multimode microplate readers. Each experiment was repeated three times, and the results were expressed as the mean percentage of cell viability relative to untreated cells.

RESULTS AND DISCUSSION

Characterization of Ag-MSNs. Ag-MSNs were prepared by a one-step synthesis, compared with previous work; there was no need for prior synthesis of Ag NPs, making it a facile and convenient method.[25,38,39] After decorating with Ag NPs, the UV absorbance of MSNs at 411 nm was enhanced and the zeta potential became positive (Supporting Information (SI) Figure S1 and S4), which indicated the successful modification of Ag NPs in MSNs. The typical morphology of Ag-MSNs was revealed distinctively through SEM. The synthesized Ag-MSNs are spherical particles with 150−300 nm in diameter (Figure 2a and SI Figure S3a). The EDX elemental analysis of Ag-MSNs was acquired using a component attachment of TEM instrument. Peaks of Ag and Si were recorded in Figure 2b, which confirmed the presence of Ag in Ag-MSNs.

HRTEM analysis was performed to study the nanostructures of Ag-MSNs at the lattice plane level. A long-range ordered streak structural feature and hexagonal array, which is the typical mesoporous structure of MCM-41 type MSNs, were observed in as-prepared Ag-MSNs (Figure 2c), and the

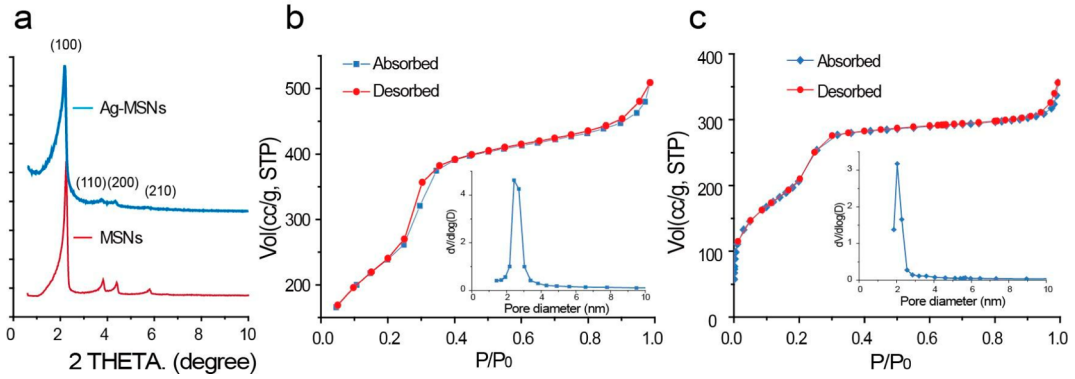

Figure 3. Characterization of Ag-MSNs: (a) the XRD pattern of the sample. (b) Nitrogen adsorption−desorption isotherms obtained at 77 K and the corresponding pore size distribution of MSNs. (c) Nitrogen adsorption−desorption isotherms obtained at 77 K and the corresponding pore size distribution of Ag-MSNs.

diameter of decorated Ag NPs is 2−10 nm (SI Figure S3b), smaller than most of those previously reported.[21,38] The CTAB, which plays the role of template and surfactant, has to be removed to avoid cellular toxicity in biological applications, and the circumfluence extraction method using chlorohydric acid and ammonium nitrate was applied to remove CTAB. This method is mild and allows Ag NPs to still remain dispersed in MSNs. After the removal of CTAB, the ordered porous structure of Ag-MSNs and uniformly dispersed Ag NPs in the framework could still be observed by HRTEM (Figure 2 b,c). Compared to the commonly used method (calcination for CTAB remove), circumfluence extraction can maintain the morphology of Ag NPs on the surface of MSNs when removing CTAB (SI Figure S5). Therefore, Ag NPs can be protected from agglomeration and release Ag ions steadily over an extended period.

XRD pattern exhibits at least four sharp Bragg peaks ((100), (110), (200), and (210)), and the strong peak around 2.2°, indicating that the ordered mesoporosity is maintained after Ag NP decoration (Figure 3a). The full width at half-maximum intensity (fwhm) is related to the order of the mesoporous materials. In this case, the fwhm of the pattern is 0.40°, which is larger than that in XRD of MSNs (0.16°). The results show that the Ag-MSNs maintain ordered structure, but the order is decreased.

The mesoporous structures of Ag-MSNs are further confirmed by nitrogen adsorption and desorption isotherms (Figure 3c), which can be classified as type IV isotherms according to the IUPAC nomenclature.[40,41] A linear increase of absorbed volume at low pressures is followed by a steep increase in nitrogen uptake at relative pressures in the range between $0.2 < p/p_0 < 0.3$, which is due to capillary condensation inside the mesopores. The long plateau at higher relative pressures indicates that pore-filling is restricted to the inflection point at $p/p_0 = 0.3$. A second steep increase occurs in nitrogen uptake and an adsorbed hysteresis loop appears at the relative pressure between $0.9 < p/p_0 < 1.0$. The corresponding pore size distribution curve (inset in Figure 3c) obtained by the Barrett−Joynerr−Halenda (BJH) method using the adsorption branch of the isotherm is centered at about 2 nm, which should result from the removed CTAB template and corroborate with the TEM results. The extracted Ag-MSNs sample has a Brumauer−Emmet−Teller (BET) specific surface area of 753 m^2g^{-1} and a single point adsorption total pore volume of 0.55 $cm^3\ g^{-1}$ estimated from the single-point amount adsorbed at $P/P_0 = 0.99$. The specific surface area and pore volume of Ag-MSNs are lower than those of purified MCM-41 (1146.495 $m^2\ g^{-1}$, 0.85 $cm^3\ g^{-1}$, Figure 3b),[35] which may provide evidence that Ag NPs are in the interior of MCM-41.

Antibacterial Activity. Silver is well-known for its strong inhibitory and bactericidal effects.[42,43] To detect the antibacterial effect of Ag-MSNs, the growth kinetics of Gram-negative bacteria *E. coli* and Gram-positive bacteria *S. aureus* in liquid media was studied (Figure 4). Bacterial growth was monitored by measuring the optical density at 600 nm (OD_{600}) based on the turbidity of the cell suspension. For these experiments, bacteria were grown to an $OD_{600} = 0.1$, and then mixed with various concentrations of the Ag-MSNs. Ag-MSNs (Ag content is 0.84 μg/mL) at a concentration of 20 μg/mL could slightly slow down the growth of *E. coli* within several hours, 40 μg/mL of Ag-MSNs (Ag content is 1.68 μg/mL) can significantly inhibit the growth of *E. coli* in 24 h and before the bacteria starts to grow. When the concentration of Ag-MSNs reached 80 μg/mL (Ag content is 3.36 μg/mL), the growth of *E. coli* can be completely inhibited (99.99% of *E. coli* was killed by the first 2 h, SI Figure S7). As *S. aureus* has a thicker cell wall than Gram-negative bacteria *E. coli*, it requires higher Ag dose to inhibit the growth of *S. aureus*.[44] In our experiment, the growth of *S. aureus* significantly decreased when the concentration of Ag-MSNs reached 160 μg/mL (Ag content is 6.72 μg/mL). When the concentration of Ag-MSNs increased to 320 μg/mL (Ag content is 13.44 μg/mL), the growth of *S. aureus* can be completely inhibited (99.99% of *S. aureus* is killed in the first 2 h, SI Figure S7). In our study, the effective concentration of Ag-MSNs is lower than that of

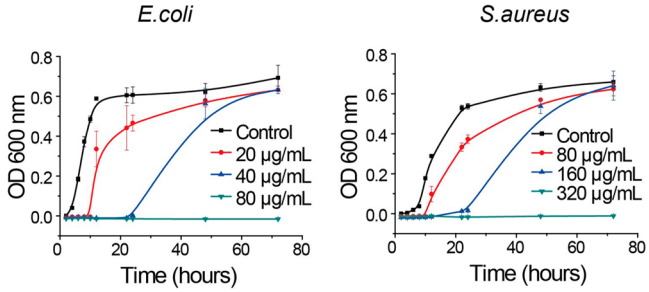

Figure 4. Concentration effects of Ag-MSNs on the growth of *E. coli* and *S. aureus*. Each data bar represents an average of three parallel samples and error bars indicate 1 standard deviation from the mean.

previously reported Ag−Si nanocomposites (which is typically 100−1000 μg/mL for *E. coli* and 1000−2000 μg/mL for *S. aureus*)[25,45−47] and commercial Ag NPs (SI Figure S6), the Ag-MSNs exhibit an excellent antibacterial activity in Gram-negative bacteria *E. coli* and Gram-positive bacteria *S. aureus*.

To further show the advantages of Ag-MSNs, we compared the antibacterial properties of Ag-MSNs with other two different Ag-containing materials (commercial Ag NPs and $AgNO_3$) by measuring the viability of bacteria. Ag MSNs, Ag NPs, and $AgNO_3$ with the same Ag concentration (3.36 μg/mL for *E. coli* and 13.44 μg/mL for *S. aureus*) were added to the molten LB-agar media and the mixtures were solidified at room temperature. LB-agar plates contained no drugs and MSNs used as controls. The suspension of *E. coli* or *S. aureus* was spread onto these plates and incubated at 37 °C. After 24 h incubation, the formation of colonies for both strains appeared in plates containing Ag NPs, $AgNO_3$, and MSNs, as well as controls. However, the presence of Ag-MSNs in the LB-agar plates could completely inhibit the formation of colonies for both types of bacteria (Figure 5). The effect was more

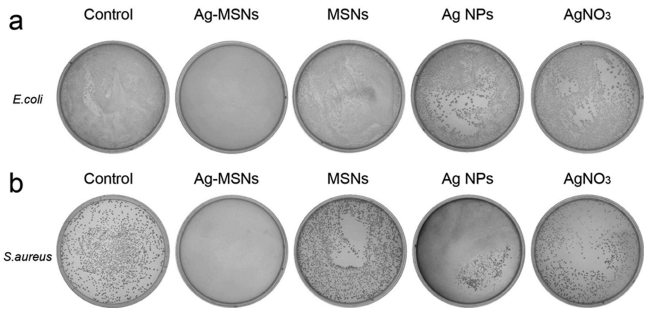

Figure 5. Antibacterial activities of Ag-MSNs, MSNs, commercial Ag NPs, and $AgNO_3$ after incubation with 1×10^5 CFU/mL bacteria for 24 h. The Ag content of Ag-MSNs, $AgNO_3$, and commercial Ag NPs is 3.36 μg/mL for *E. coli* and 13.44 μg/mL for *S. aureus*. Petri dishes with LB-agar inoculated with (a) *E. coli* and (b) *S. aureus*, showing different numbers of colonies formed when treated with different materials.

pronounced when the incubation time was prolonged to 3 days, where there was still no colony for both types of bacteria in the plate contained Ag-MSNs, but much more formation of bacterial colonies in plates containing other Ag materials (SI Figure S8). In our 30-day test (proven to be long enough to prevent implants from postinfection in the early, intermediate, and late stages[48]), the antibacterial ability of Ag-MSNs was maintained and there was no colony formation. Similar results were also identified by turbidity measurements. Ag-MSNs, commercial Ag NPs, and $AgNO_3$ with same Ag content (3.36 μg/mL for *E. coli* and 13.44 μg/mL for *S. aureus*) were incubated with 1×10^6 CFU/mL both types of bacteria in LB media and the turbidity was measured at different time points. The samples with MSNs became turbid in 12 h, which is the same as the control group. Ag-MSNs could completely inhibit the growth of both *E. coli* and *S. aureus* (SI Figure S8). In contrast, AgNPs and $AgNO_3$ with the same silver content could only delay bacterial growth in 24 h, and both types of bacteria proliferated within 48 h. The silver salts or nanoparticles are easily aggregated in media by interact with the complex component and resulted in a loss of or a short time of antibacterial activity.[5,45] We believe that the much improved effect of the Ag-MSNs over time is because the supporting matrix MCM-41 type MSNs could protect the silver NPs from aggregation and enables continuous release of Ag ions.

Antibacterial Mechanisms of Ag-MSNs. To explore the mechanisms of Ag-MSNs with remarkable antibacterial effects, we compared the morphological changes of Ag-MSNs and commercial Ag NPs after incubation with bacteria for 1−30 days. After 1 day incubation, the LB liquid media containing bacteria (either *E. coli* or *S. aureus*) and Ag-MSNs (3.36 μg/mL for *E. coli* and 13.44 μg/mL for *S. aureus*, in terms of Ag element) remained transparent, while the mixtures containing Ag NPs (the same Ag element to Ag-MSNs) and bacteria became turbid. STEM images suggested that Ag-MSNs can adhere to bacteria (either *E. coli* or *S. aureus*). In addition, the decorated Ag NPs are still highly dispersed in the framework of MCM-41 type MSNs (Figure 6a), and compared to the

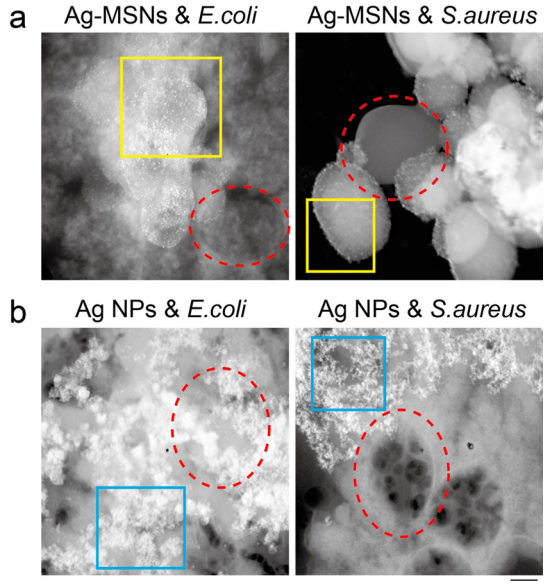

Figure 6. STEM images of Ag-MSNs and commercial Ag NPs after incubation with *E. coli* or *S. aureus* for 24 h. (a) Small Ag NPs were highly dispersed in the framework of MSNs after incubation with *E. coli* or *S. aureus*; (b) Ag NPs aggregated when incubated with *E. coli* or *S. aureus*; scale bar = 200 nm. Red dashed circles highlight the bacteria (either *E. coli* or *S. aureus*). Yellow boxes highlight MSNs decorated with highly dispersed Ag NPs. Blue boxes represent aggregated Ag NPs.

primary synthesized Ag-MSNs, there is little morphological change (SI Figure S2a). More importantly, these highly dispersed Ag-MSNs can stably release Ag ions over a course of 30 days (Figure 7). In contrast, although Ag NPs can adhere to bacteria, they aggregated seriously on the surface of bacteria or in the media (Figure 6b), their states of dispersion significantly changed compared to their initial morphology (SI Figure S2b). In fact, bacteria often carry negative charges (also proven in our experiments, SI Figure S4), and they can easily adhere to materials carrying positive charges.[49] In addition, Ag NPs with small size and highly dispersed state can release large amounts of Ag ions; therefore, they can exhibit strong antibacterial activity at early stage. However, with the extension of the time, the leakage of the already dead bacteria or the complex culture media often causes the aggregation of Ag NPs. The aggregated Ag NPs release fewer Ag ions than the highly dispersed ones (SI Figure S10), so the bacteria that survive at the early stage begin to multiply and cause the loss of

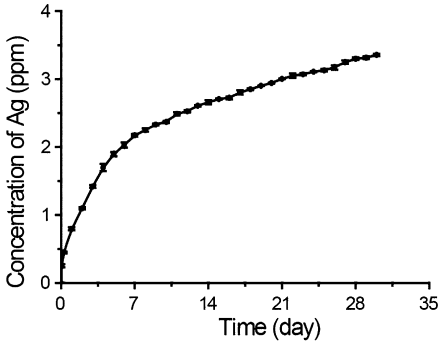

Figure 7. Release of silver ions from Ag-MSNs at 37 °C. Ag-MSNs can continuously release Ag ions.

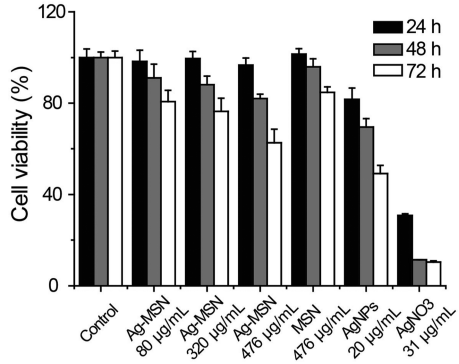

Figure 8. Cytotoxicity of Ag-MSNs on HUVEC. Concentrations of Ag element in Ag-MSNs (476 μg/mL), Ag NPs (20 μg/mL), and Ag NO_3 (31 μg/mL) are 20 μg/mL. Experiments were performed in triplicate; values represent the relative viability compared to untreated cells as means ± SEM of one representative experiment (n = 3).

antibacterial activity.[50,51] In our experiments, the highly dispersed Ag NPs can sustain at least 30 days (SI Figure S12) and the Ag ions can be continuously released into media to inhibit the growth of bacteria.

Our experiments demonstrate that the Ag-MSNs exhibit enhanced antibacterial activity in both *E. coli* and *S. aureus*, and it is closely related to their structure (uniformly distributed Ag NPs), surface charge (positive charges), and size (2−10 nm). Previous studies have summarized several possible antibacterial mechanisms of Ag NPs:[52] Ag NPs will release Ag^+ ions which can interact with thiol groups of vital proteins, which will result in inactivation of enzyme proteins and disruption of respiration. This is often considered as the main mechanism of the antimicrobial activity of Ag NPs. The release rate of Ag^+ ions depends in part on the size of Ag NPs; the Ag NPs with smaller size might induce faster Ag^+ ion release.[53] In actual application, the complex cultural environment and the dead bacteria often cause the aggregation of Ag NPs, whose larger size reduced the release of Ag^+ ions, leading to the decrease or loss of antibacterial activity. In our study, the Ag NPs decorated in MCM-41 type MSNs can effectively prevent aggregation and thus retain good dispersity in the culture media. The well-dispersed distribution of Ag NPs makes Ag ions release steadily from MSNs over a long period and ultimately realize long-term antibacterial effects. Besides, the positively charged Ag-MSNs make them adhere to the surface of negatively charged bacteria easily.[54,55] In most cases, the diameter of Ag NPs in silica materials ranges from 20 to 50 nm;[45,56] however, in our study the Ag NPs in MCM-41 type MSNs carrier is only 2−10 nm, which contributes their increased antibacterial effects. Compared to larger Ag NPs, they may have a faster release of Ag ions, thus inducing higher toxicity to bacteria.[43]

Cellular Toxicology Evaluation. Silver salts or nanoparticles can cause damage to mitochondria, DNA, and increase reactive oxygen species, leading to cell death.[45,57] Silica materials are proven to have good biocompatibility and have broad applications in biomedicine.[58,59] The in vitro cytotoxicity of the Ag-MSNs was evaluated on human umbilical vein endothelial cells (HUVEC, a common cell line to evaluate the cytotoxicity of materials[36,60,61]) using a CCK kit. The antibacterial concentration of Ag-MSNs (80 and 320 μg/mL) showed no obvious cytotoxicity within 24 h, which is similar to that of MSNs (Figure 8). Even if the concentration of Ag-MSNs is increased to 476 μg/mL (Ag content is 20 μg/mL), the cell viability is still more than 90%. The cell viabilities of the above groups were higher than 60% after 72 h of incubation. By contrast, Ag NPs and $AgNO_3$ containing the same amount of silver to Ag-MSNs showed significant toxicology. The viability of cells treated with Ag NPs was decreased to 79%, while that of cells treated with $AgNO_3$ was only 30% within 24 h. After the 72 h incubation, the cell viability dropped below 50%. These results indicated that Ag-MSNs not only have a strong bactericidal effect on both Gram-negative and Gram-positive bacteria, but they also have better biocompatibility than commercial Ag NPs or $AgNO_3$.

CONCLUSIONS

We describe the synthesis of Ag-MSNs via the co-condensation method in diluted sodium hydroxide solution. The Ag NPs with small sizes have high density and well-dispersed distribution in the framework of MCM-41 type MSNs. This structure can protect Ag NPs from aggregation and allow Ag ions to continuously release from the MSNs vectors. Thus, Ag-MSNs show long-term antibacterial activity on Gram-negative and Gram-positive bacteria at a low concentration. More importantly, these nanoparticles have good biocompatibility. In summary, Ag-MSNs have great potential application in biomedicine as multifunctional NPs, especially showing long-term antibacterial effect for practical applications.

ASSOCIATED CONTENT

Supporting Information

Characterizations of Ag-MSNs and MSNs with UV−vis spectrometer and zeta potential are provided. Zeta potential of *E. coli* and *S. aureus*, TEM of Ag-MSNs after calcination, STEM images of Ag-MSNs and Ag NPs, bactericidal curve of Ag-MSNs, Ag^+ release rate of Ag-MSNs and Ag NPs in LB medium, STEM images of Ag-MSNs at different time points are also provided. This material is available free of charge via the Internet at http://pubs.acs.org.

AUTHOR INFORMATION

Corresponding Authors

*Tel: +86-10-82545558. E-mail: xingyujiang@nanoctr.cn.
*E-mail: zhangwei@nanoctr.cn.
*E-mail: caiqiang@mail.tsinghua.edu.cn.

Author Contributions

The manuscript was written through contributions of all authors. All authors have given approval to the final version of the manuscript. Yue Tian and Juanjuan Qi contributed equally.

Notes

The authors declare no competing financial interest.

■ ACKNOWLEDGMENTS

We acknowledge Ministry of Science and Technology (2012AA022703, 2012AA030308), the Ministry of Health P.R.China (2012ZX10001-008), the Chinese Academy of Science (NNCAS-2010-5 & XDA09030305), and the National Science Foundation of China (21025520, 21222502, 51373043, 21105018 & 81361140345), and Beijing Municipal Science & Technology Commission (Z131100002713024). We thank Department of Materials Science and Engineering of Tsinghua University for electron microscopy analysis.

■ REFERENCES

(1) Chernousova, S.; Epple, M. Silver as Antibacterial Agent: Ion, Nanoparticle, and Metal. *Angew. Chem., Int. Ed.* **2013**, *52*, 1636−1653.
(2) Lemire, J. A.; Harrison, J. J.; Turner, R. J. Antimicrobial Activity of Metals: Mechanisms, Molecular Targets and Applications. *Nat. Rev. Microbiol.* **2013**, *11*, 371−384.
(3) Han, E.; Wu, D.; Qi, S.; Tian, G.; Niu, H.; Shang, G.; Yan, X.; Yang, X. Incorporation of Silver Nanoparticles into the Bulk of the Electrospun Ultrafine Polyimide Nanofibers via a Direct Ion Exchange Self-Metallization Process. *ACS Appl. Mater. Interfaces* **2012**, *4*, 2583−2590.
(4) Barras, A.; Martin, F. A.; Bande, O.; Baumann, J.-S.; Ghigo, J.-M.; Boukherroub, R.; Beloin, C.; Siriwardena, A.; Szunerits, S. Glycan-Functionalized Diamond Nanoparticles as Potent E. coli Anti-Adhesives. *Nanoscale* **2013**, *5*, 2307−2316.
(5) Lok, C. N.; Ho, C. M.; Chen, R.; He, Q. Y.; Yu, W. Y.; Sun, H. Z.; Tam, P. H.; Chiu, J. F.; Che, C. M. Silver Nanoparticles: Partial Oxidation and Antibacterial Activities. *J. Biol. Inorg. Chem.* **2007**, *12*, 527−534.
(6) Pal, S.; Tak, Y. K.; Song, J. M. Does the Antibacterial Activity of Silver Nanoparticles Depend on the Shape of the Nanoparticle? A Study of the Gram-Negative Bacterium Escherichia coli. *Appl. Environ. Microbiol.* **2007**, *73*, 1712−1720.
(7) Aruguete, D. M.; Kim, B.; Hochella, M. F.; Ma, Y.; Cheng, Y.; Hoegh, A.; Liu, J.; Pruden, A. Antimicrobial Nanotechnology: Its Potential for the Effective Management of Microbial Drug Resistance and Implications for Research Needs in Microbial Nanotoxicology. *Environ. Sci.: Processes Impacts* **2013**, *15*, 93−102.
(8) Kawahara, K.; Tsuruda, K.; Morishita, M.; Uchida, M. Antibacterial Effect of Silver-Zeolite on Oral Bacteria Under Anaerobic Conditions. *Dent. Mater.* **2000**, *16*, 452−455.
(9) Zhang, L.; Yu, J. C.; Yip, H. Y.; Li, Q.; Kwong, K. W.; Xu, A. W.; Wong, P. K. Ambient Light Reduction Strategy to Synthesize Silver Nanoparticles and Silver-Coated TiO_2 with Enhanced Photocatalytic and Bactericidal Activities. *Langmuir* **2003**, *19*, 10372−10380.
(10) Perkas, N.; Lipovsky, A.; Amirian, G.; Nitzan, Y.; Gedanken, A. Biocidal Properties of TiO_2 Powder Modified with Ag Nanoparticles. *J. Mater. Chem. B* **2013**, *1*, 5309−5316.
(11) Zhang, S.; Fu, R.; Wu, D.; Xu, W.; Ye, Q.; Chen, Z. Preparation and Characterization of Antibacterial Silver-Dispersed Activated Carbon Aerogels. *Carbon* **2004**, *42*, 3209−3216.
(12) Ōya, A.; Banse, T.; Ohashi, F.; Ōtani, S. An Antimicrobial and Antifungal Agent Derived from Montmorillonite. *Appl. Clay Sci.* **1991**, *6*, 135−142.
(13) Rhodes, K. H.; Davis, S. A.; Caruso, F.; Zhang, B.; Mann, S. Hierarchical Assembly of Zeolite Nanoparticles into Ordered Macroporous Monoliths Using Core−Shell Building Blocks. *Chem. Mater.* **2000**, *12*, 2832−2834.
(14) Long, T. C.; Saleh, N.; Tilton, R. D.; Lowry, G. V.; Veronesi, B. Titanium Dioxide (P25) Produces Reactive Oxygen Species in Immortalized Brain Microglia (BV2): Implications for Nanoparticle Neurotoxicity. *Environ. Sci. Technol.* **2006**, *40*, 4346−4352.
(15) Xue, B.; Chen, P.; Hong, Q.; Lin, J.; Tan, K. L. Growth of Pd, Pt, Ag and Au Nanoparticles on Carbon Nanotubes. *J. Mater. Chem.* **2001**, *11*, 2378−2381.
(16) Dong, R. X.; Chou, C. C.; Lin, J. J. Synthesis of Immobilized Silver Nanoparticles on Ionic Silicate Clay and Observed Low-Temperature Melting. *J. Mater. Chem.* **2009**, *19*, 2184−2188.
(17) Kresge, C. T.; Leonowicz, M. E.; Roth, W. J.; Vartuli, J. C.; Beck, J. S. Ordered Mesoporous Molecular Sieves Synthesized by a Liquid-Crystal Template Mechanism. *Nature* **1992**, *359*, 710−712.
(18) Slowing, I. I.; Trewyn, B. G.; Lin, V. S. Y. Mesoporous Silica Nanoparticles for Intracellular Delivery of Membrane-Impermeable Proteins. *J. Am. Chem. Soc.* **2007**, *129*, 8845−8849.
(19) Angelos, S.; Khashab, N. M.; Yang, Y. W.; Trabolsi, A.; Khatib, H. A.; Stoddart, J. F.; Zink, J. I. pH Clock-Operated Mechanized Nanoparticles. *J. Am. Chem. Soc.* **2009**, *131*, 12912−12914.
(20) Klichko, Y.; Liong, M.; Choi, E.; Angelos, S.; Nel, A. E.; Stoddart, J. F.; Tamanoi, F.; Zink, J. I. Mesostructured Silica for Optical Functionality, Nanomachines, and Drug Delivery. *J. Am. Ceram. Soc.* **2009**, *92*, S2−S10.
(21) Li, Z.; Barnes, J. C.; Bosoy, A.; Stoddart, J. F.; Zink, J. I. Mesoporous Silica Nanoparticles in Biomedical Applications. *Chem. Soc. Rev.* **2012**, *41*, 2590−2605.
(22) Taylor, K. M. L.; Kim, J. S.; Rieter, W. J.; An, H.; Lin, W.; Lin, W. Mesoporous Silica Nanospheres as Highly Efficient MRI Contrast Agents. *J. Am. Chem. Soc.* **2008**, *130*, 2154−2155.
(23) Vivero Escoto, J. L.; Slowing, I. I.; Wu, C. W.; Lin, V. S. Y. Photoinduced Intracellular Controlled Release Drug Delivery in Human Cells by Gold-Capped Mesoporous Silica Nanosphere. *J. Am. Chem. Soc.* **2009**, *131*, 3462−3463.
(24) Trewyn, B. G.; Slowing, I. I.; Giri, S.; Chen, H. T.; Lin, V. S. Y. Synthesis and Functionalization of a Mesoporous Silica Nanoparticle Based on the Sol−Gel Process and Applications in Controlled Release. *Acc. Chem. Res.* **2007**, *40*, 846−853.
(25) Liong, M.; France, B.; Bradley, K. A.; Zink, J. I. Antimicrobial Activity of Silver Nanocrystals Encapsulated in Mesoporous Silica Nanoparticles. *Adv. Mater.* **2009**, *21*, 1684−1689.
(26) Hu, Y.; Cai, K.; Luo, Z.; Jandt, K. D. Layer-by-Layer Assembly of β-Estradiol Loaded Mesoporous Silica Nanoparticles on Titanium Substrates and Its Implication for Bone Homeostasis. *Adv. Mater.* **2010**, *22*, 4146−4150.
(27) Ouarda, F.; Rupak, K. S.; Manash, R. D.; Ratul, S.; Lionel, M.; Yannick, C.; Toufik, H.; Mustapha, M.; Rabah, B. The Antimicrobial Effect of Silicon Nanowires Decorated with Silver and Copper Nanoparticles. *Nanotechnology* **2013**, *24*, 495101.
(28) Bharali, D. J.; Klejbor, I.; Stachowiak, E. K.; Dutta, P.; Roy, I.; Kaur, N.; Bergey, E. J.; Prasad, P. N.; Stachowiak, M. K. Organically Modified Silica Nanoparticles: a Nonviral Vector for In Vivo Gene Delivery and Expression in the Brain. *Proc. Natl. Acad. Sci. U.S.A.* **2005**, *102*, 11539−11544.
(29) Trewyn, B. G.; Whitman, C. M.; Lin, V. S. Y. Morphological Control of Room-Temperature Ionic Liquid Templated Mesoporous Silica Nanoparticles for Controlled Release of Antibacterial Agents. *Nano Lett.* **2004**, *4*, 2139−2143.
(30) Rocks, L.; Faulds, K.; Graham, D. Rationally Designed SERS Active Silica Coated Silver Nanoparticles. *Chem. Commun.* **2011**, *47*, 4415−4417.
(31) Uzayisenga, V.; Lin, X. D.; Li, L. M.; Anema, J. R.; Yang, Z. L.; Huang, Y. F.; Lin, H. X.; Li, S. B.; Li, J. F.; Tian, Z. Q. Synthesis, Characterization, and 3D-FDTD Simulation of Ag@SiO_2 Nanoparticles for Shell-Isolated Nanoparticle-Enhanced Raman Spectroscopy. *Langmuir* **2012**, *28*, 9140−9146.
(32) Hornebecq, V.; Antonietti, M.; Cardinal, T.; Treguer-Delapierre, M. Stable Silver Nanoparticles Immobilized in Mesoporous Silica. *Chem. Mater.* **2003**, *15*, 1993−1999.
(33) Gu, G.; Xu, J.; Wu, Y.; Chen, M.; Wu, L. Synthesis and Antibacterial Property of Hollow SiO_2/Ag Nanocomposite Sheres. *J. Colloid Interface Sci.* **2011**, *359*, 327−333.

(34) Samberg, M. E.; Orndorff, P. E.; Monteiro-Riviere, N. A. Antibacterial Efficacy of Silver Nanoparticles of Different Sizes, Surface Conditions and Synthesis Methods. *Nanotoxicology* **2011**, *5*, 244−253.
(35) Cai, Q.; Luo, Z. S.; Pang, W. Q.; Fan, Y. W.; Chen, X. H.; Cui, F. Z. Dilute Solution Routes to Various Controllable Morphologies of MCM-41 Silica with a Basic Medium. *Chem. Mater.* **2001**, *13*, 258−263.
(36) Zhao, Y.; Chen, Z.; Chen, Y.; Xu, J.; Li, J.; Jiang, X. Synergy of Non-antibiotic Drugs and Pyrimidinethiol on Gold Nanoparticles against Superbugs. *J. Am. Chem. Soc.* **2013**, *135*, 12940−12943.
(37) Zhao, Y.; Tian, Y.; Cui, Y.; Liu, W.; Ma, W.; Jiang, X. Small Molecule-Capped Gold Nanoparticles as Potent Antibacterial Agents That Target Gram-Negative Bacteria. *J. Am. Chem. Soc.* **2010**, *132*, 12349−12356.
(38) Saint-Cricq, P.; Wang, J.; Sugawara-Narutaki, A.; Shimojima, A.; Okubo, T. A New Synthesis of Well-Dispersed, Core-Shell Ag@SiO_2 Mesoporous Nanoparticles Using Amino Acids and Sugars. *J. Mater. Chem. B* **2013**, *1*, 2451−2454.
(39) Yang, H.; Liu, Y.; Shen, Q.; Chen, L.; You, W.; Wang, X.; Sheng, J. Mesoporous Silica Microcapsule-Supported Ag Nanoparticles Fabricated via Nano-Assembly and Its Antibacterial Properties. *J. Mater. Chem.* **2012**, *22*, 24132−24138.
(40) de Boer, J. H.*The Structure and Properties of Porous Materials*; Butterworths: London, 1958.
(41) Gregg, S. J.; Sing, K. S. W. *Adsorption, Surface Area, and Porosity*, 2nd ed.; Academic Press, London, 1982.
(42) Li, W. R.; Xie, X. B.; Shi, Q. S.; Zeng, H. Y.; Ou-Yang, Y. S.; Chen, Y. B. Antibacterial Activity and Mechanism of Silver Nanoparticles on Escherichia coli. *Appl. Microbiol. Biotechnol.* **2010**, *85*, 1115−1122.
(43) Xiu, Z. M.; Zhang, Q. B.; Puppala, H. L.; Colvin, V. L.; Alvarez, P. J. J. Negligible Particle-Specific Antibacterial Activity of Silver Nanoparticles. *Nano Lett.* **2012**, *12*, 4271−4275.
(44) Feng, Q. L.; Wu, J.; Chen, G. Q.; Cui, F. Z.; Kim, T. N.; Kim, J. O. A Mechanistic Study of the Antibacterial Effect of Silver Ions on Escherichia coli and Staphylococcus aureus. *J. Biomed. Mater. Res.* **2000**, *52*, 662−668.
(45) Ma, Z.; Ji, H.; Tan, D.; Teng, Y.; Dong, G.; Zhou, J.; Qiu, J.; Zhang, M. Silver Nanoparticles Decorated, Flexible SiO_2 Nanofibers with Long-Term Antibacterial Effect as Reusable Wound Cover. *Colloids Surf., A* **2011**, *387*, 57−64.
(46) Egger, S.; Lehmann, R. P.; Height, M. J.; Loessner, M. J.; Schuppler, M. Antimicrobial Properties of a Novel Silver-Silica Nanocomposite Material. *Appl. Environ. Microbiol.* **2009**, *75*, 2973−2976.
(47) Kim, Y. H.; Lee, D. K.; Cha, H. G.; Kim, C. W.; Kang, Y. S. Synthesis and Characterization of Antibacterial Ag−SiO_2 Nanocomposite. *J. Phys. Chem. C* **2007**, *111*, 3629−3635.
(48) Zhao, L.; Wang, H.; Huo, K.; Cui, L.; Zhang, W.; Ni, H.; Zhang, Y.; Wu, Z.; Chu, P. K. Antibacterial Nano-Structured Titania Coating Incorporated with Silver Nanoparticles. *Biomaterials* **2011**, *32*, 5706−5716.
(49) Zhao, Y.; Jiang, X. Multiple Strategies to Activate Gold Nanoparticles as Antibiotics. *Nanoscale* **2013**, *5*, 8340−8350.
(50) Morones, J. R.; Elechiguerra, J. L.; Camacho, A.; Holt, K.; Kouri, J. B.; Ramirez, J. T.; Yacaman, M. J. The Bactericidal Effect of Silver Nanoparticles. *Nanotechnology* **2005**, *16*, 2346−2353.
(51) Chen, X.; Schluesener, H. J. Nanosilver: a Nanoproduct in Medical Application. *Toxicol. Lett.* **2008**, *176*, 1−12.
(52) Reidy, B.; Haase, A.; Luch, A.; Dawson, K.; Lynch, I. Mechanisms of Silver Nanoparticle Release, Transformation and Toxicity: a Critical Review of Current Knowledge and Recommendations for Future Studies and Applications. *Materials* **2013**, *6*, 2295−2350.
(53) Zhang, W.; Yao, Y.; Sullivan, N.; Chen, Y. Modeling the Primary Size Effects of Citrate-Coated Silver Nanoparticles on Their Ion Release Kinetics. *Environ. Sci. Technol.* **2011**, *45*, 4422−4428.
(54) Zhang, L.; Dhillon, P.; Yan, H.; Farmer, S.; Hancock, R. E. W. Interactions of Bacterial Cationic Peptide Antibiotics with Outer and Cytoplasmic Membranes ofPseudomonas aeruginosa. *Antimicrob. Agents Chemother.* **2000**, *44*, 3317−3321.
(55) Li, L. l.; Wang, H. Antibacterial Agents: Enzyme-Coated Mesoporous Silica Nanoparticles as Efficient Antibacterial Agents In Vivo. *Adv. Healthcare Mater.* **2013**, *2*, 1298−1298.
(56) Zienkiewicz Strzałka, M.; Pasieczna Patkowska, S.; Kozak, M.; Pikus, S. Silver Nanoparticles Incorporated onto Ordered Mesoporous Silica from Tollen's Reagent. *Appl. Surf. Sci.* **2013**, *266*, 337−343.
(57) Carlson, C.; Hussain, S. M.; Schrand, A. M.; K. Braydich Stolle, L.; Hess, K. L.; Jones, R. L.; Schlager, J. J. Unique Cellular Interaction of Silver Nanoparticles: Size-Dependent Generation of Reactive Oxygen Species. *J. Phys. Chem. B* **2008**, *112*, 13608−13619.
(58) Zhong, Y.; Peng, F.; Bao, F.; Wang, S.; Ji, X.; Yang, L.; Su, Y.; Lee, S. T.; He, Y. Large-Scale Aqueous Synthesis of Fluorescent and Biocompatible Silicon Nanoparticles and Their Use as Highly Photostable Biological Probes. *J. Am. Chem. Soc.* **2013**, *135*, 8350−8356.
(59) Sotiriou, G. A.; Franco, D.; Poulikakos, D.; Ferrari, A. Optically Stable Biocompatible Flame-Made SiO_2-Coated Y_2O_3:Tb^{3+} Nanophosphors for Cell Imaging. *ACS Nano* **2012**, *6*, 3888−3897.
(60) Hu, C.-M. J.; Fang, R. H.; Copp, J.; Luk, B. T.; Zhang, L. A Biomimetic Nanosponge that Absorbs Pore-Forming Toxins. *Nat. Nanotechnol.* **2013**, *8*, 336−340.
(61) Tian, Y.; Wang, H.; Liu, Y.; Mao, L.; Chen, W.; Zhu, Z.; Liu, W.; Zheng, W.; Zhao, Y.; Kong, D.; Yang, Z.; Zhang, W.; Shao, Y.; Jiang, X. A Peptide-Based Nanofibrous Hydrogel as a Promising DNA Nanovector for Optimizing the Efficacy of HIV Vaccine. *Nano Lett.* **2014**, *14*, 1439−1445.